ACS APPLIED ELECTRONIC MATERIALS

pubs.acs.org/acsaelm

Article

Synthesis and Characterization of Nitrogen-Doped Crystallized SiC Films from Liquid Precursors

Benedikt Fischer,* Maurice Nuys, Stefan Haas, Oliver Thimm, Gunnar Schöpe, Pascal Foucart, Astrid Besmehn, and Uwe Rau

Cite This: https://doi.org/10.1021/acsaelm.4c01992

Read Online

ACCESS | Metrics & More | Article Recommendations | Supporting Information

ABSTRACT: Silicon carbide (SiC) is an established material for photovoltaics and other semiconductor devices due to its wide band gap and high thermal stability. Traditional deposition systems for thin, doped SiC layers are often costly and complex. This study investigates the use of 1,4-disilabutane as a low-cost liquid precursor with a rather low decomposition temperature for the deposition of hydrogenated amorphous silicon carbide (a-SiC:H) films at atmospheric pressure. Nitrogen doping was achieved using 1,1,3,3-tetramethyldisilazane. The films were characterized by Fourier-transform infrared spectroscopy, Raman spectroscopy, secondary ion mass spectrometry, and conductivity measurements. Optimizing the deposition temperature maximized the Si−C bond density. Crystallization was induced by annealing at temperatures between 800 and 1100 °C, resulting in a three-order-of-magnitude increase in conductivity. The highest conductivity achieved was 0.03 S cm^{-1} for crystalline, N-doped SiC films. This cost-effective method for producing highly conductive, crystalline SiC films offers significant potential for industrial applications.

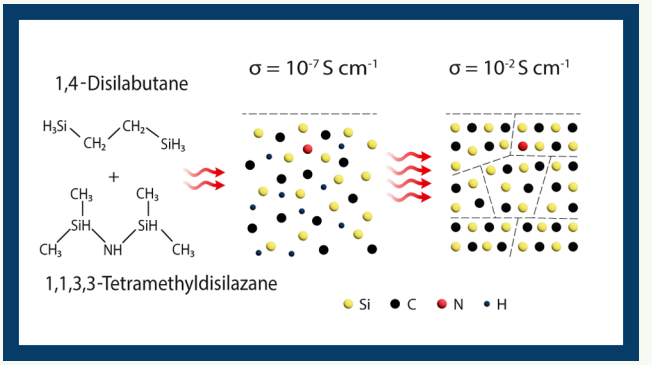

KEYWORDS: *amorphous silicon carbide, disilabutane, pyrolysis, crystallization, doping, atmospheric pressure deposition, conductivity*

INTRODUCTION

Silicon carbide (SiC) distinguishes itself with a wide band gap and exceptional chemical and thermal stability, setting it apart from silicon. These characteristics allow SiC to function efficiently under extreme conditions like high temperatures and voltages, making it a prime choice for next-generation electronic and photovoltaic devices.[1−3] In the photovoltaic industry, high-efficiency silicon solar cells, such as TOPCon (Tunnel Oxide Passivated Contact) and all-silicon tandem solar cells, benefit significantly from materials like SiC that offer high electrical conductivity, hereafter referred to as conductivity, excellent passivation and robust thermal stability.[4−7] Traditional methods for fabricating thin, doped SiC layers involve systems like plasma enhanced chemical vapor deposition, hot wire chemical vapor deposition, magnetron sputtering or molecular beam epitaxy that usually operate under high vacuum conditions.[4,6,8,9] While effective, these vacuum-based processes are often cost-prohibitive and challenging to scale for industrial applications. Therefore, there is a critical need for more cost-effective, fast and scalable methods to deposit thin, doped SiC layers at low temperatures and atmospheric pressure. This study aims to address these challenges by employing atmospheric pressure CVD (APCVD) combined with liquid precursors. Specifically, we utilize low-cost 1,4-disilabutane (DB) as the primary precursor for the deposition of hydrogenated amorphous silicon carbide (a-SiC:H) films at atmospheric pressure. Beside an improved handling, DB promises a lower temperature for thermal decomposition (~500 °C) in contrast to gaseous precursors like methylsilane (~750 °C).[10,11] Nitrogen (N) doping is achieved by adding 1,1,3,3-tetramethyldisilazane (TMD). The primary objectives are to show the feasibility of the doped SiC film deposition leveraging APCVD without the need of an ultrahigh vacuum and using low-cost liquid precursors to address key limitations of traditional vacuum-based methods. Compared to existing techniques, the proposed method is significantly more cost-effective and scalable, making it viable for large-scale industrial applications. The use of low-cost 1,4-disilabutane (DB) enables deposition at lower temperatures (~500 °C) than conventional gaseous precursors like methylsilane, reducing energy requirements and broadening material compatibility. While the method can be used to achieve a range of Si:C ratios, we optimize the deposition and

Received: November 7, 2024
Revised: January 15, 2025
Accepted: January 16, 2025

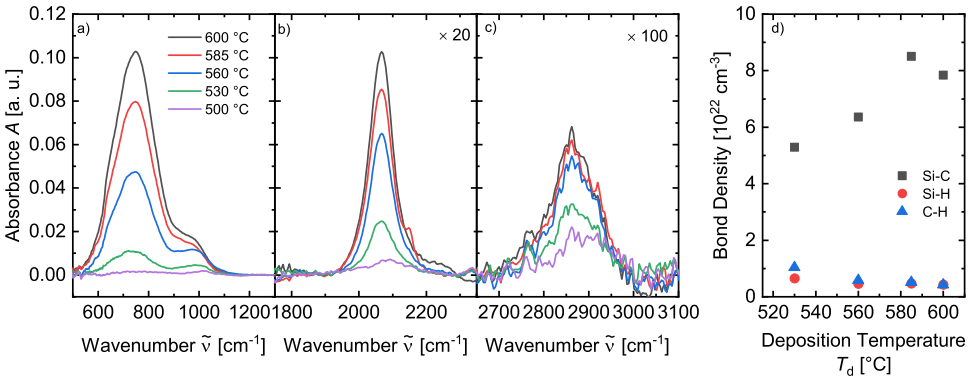

Figure 1. FTIR spectra of a-SiC:H films deposited at temperatures between 500 and 600 °C. (a) Si−H wagging, Si−C stretching, and Si−C−H_x wagging modes; (b) Si−H stretching modes; (c) C−H stretching modes; and (d) density of Si−C, Si−H, and C−H bonds as a function of the deposition temperature.

annealing temperature T_d and T_a to maximize the density of crystalline Si−C bonds. In order to ensure direct applicability of the films in electrical devices such as TOPCon solar cells or microelectronic-mechanical systems, the electrical properties of the films are being investigated and enhanced through the introduction of nitrogen doping and crystallization, resulting in conductivity improvements of up to 3 orders of magnitude.

In this study, we begin by presenting the successful deposition of a-SiC:H films at temperatures between 500 and 600 °C and the optimization of the deposition temperature to maximize the carbon concentration c_C. Next, we investigate the crystallization process induced by annealing at temperatures ranging from 800 to 1100 °C. We then discuss the effects of N doping on the conductivity of the films, demonstrating a three-order-of-magnitude increase in conductivity and achieving a maximum value of 0.03 S cm^{-1} for crystalline, N-doped SiC films. Finally, we compare our findings with existing literature and underscores the potential applications of these conductive, crystalline SiC films in nano electronics and photovoltaics.

EXPERIMENTAL DETAILS

The a-SiC:H films were deposited using an in-house made APCVD system set up in a glovebox with a N_2 atmosphere and an O_2 concentration of 1−5 ppm, as described in detail in ref 12. The system consists of a cooled inlet block and a heated deposition chamber. The inlet block has a precursor reservoir into which the required amount of precursor is dosed just prior to deposition using an Eppendorf pipet. To start the deposition process, the precursor is flushed into the deposition chamber with N_2 and sprays onto a buffer plate where it evaporates due to the elevated temperature in the deposition chamber. The vaporized precursor is then distributed within the deposition chamber and approaches the substrate, which rests on a quartz plate heated to temperatures between 500 and 600 °C. At the hot substrate surface, the precursor decomposes and reacts with the surface atoms of the substrate. The deposition process ends when the chamber is opened, and the substrates are removed from the quartz plate.

For the deposition series in this work, the films were grown for 10 min. We employed 1,4-DB as precursor for the a-SiC:H deposition and 1,1,3,3- TMD for the N-doping. Both precursors were sourced from Gelest with a purity of 99 and 97%, respectively. For the deposition of undoped a-SiC:H films, 15 μL of pure DB was used. For the doped films, we prepared a solution of 20% TMD dissolved in DB. To achieve the desired doping precursor content, we added a suitable mixture of this solution and pure DB to the precursor reservoir using an Eppendorf pipet, resulting in a total precursor amount of 15−20 μL. Due to the high volatility of the precursor, rapid injection of the precursor into the precursor reservoir is required, although this was kept at temperatures below 35 °C by a Peltier element.

The films were deposited on polished p-type high resistivity c-Si (100) float-zone wafers (525 μm, 20 Ω cm) with native oxide for Fourier-transform infrared (FTIR) spectroscopy and secondary ion mass spectrometry (SIMS) and on 1 mm quartz glass for Raman spectroscopy and conductivity measurements. Annealing of the films was conducted in a quartz-furnace with a heating rate of 6.67 °C/min and a dwell time of 120 min at the highest temperature. Prior to annealing, the furnace was flushed with N_2 under ambient conditions. Due to the absence of vacuum purging, a significant amount of residual oxygen (O_2) could have remained in the furnace during the annealing process. To remove resulting surface oxide, some samples were etched in a 1% diluted hydrofluoric (HF) acid solution for 10 min after the annealing step.

The bonding structure of the film material was analyzed using FTIR measurements in transmission mode with a Nicolet 5700 system from Thermo Electron Corporation. The bond density of Si−C, Si−H and C−H bonds were determined from corresponding stretching vibration peaks in the FTIR spectra.[13] The SiC bonding vibration at about 780−800 cm^{-1} is decomposed into the sum of a Lorentzian and Gaussian shape representing contributions from crystalline and amorphous SiC, respectively. The peaks were fitted as described in ref 14. The FTIR system gives a spectrum showing the absorbance A vs the wavenumber as output. The absorption coefficient α can be calculated by $\alpha = A \times \ln(10)/d$. The film thickness d was measured by spectroscopic ellipsometry using a T-Solar/M2000 from J.A. Woollam. To calculate α of the crystalline films we used the film thickness of the amorphous film, since the fit of the ellipsometry data of the crystallized films was less robust. This can lead to an underestimation of α due to shrinking effects of the film during annealing, e.g., Heera et al.[15] found a density difference between amorphous and crystalline SiC of 12%. To investigate the elemental in-depth distribution, SIMS depth profiles were measured using 1 kV Cs ions for sputtering (300 × 300 μm^2) and 30 kV Bi ions for analysis (40 × 40 μm^2). Measurements were performed on a ToF-SIMS5.ncs instrument (IONTOF GmbH, Muenster, Germany). Raman spectroscopy was performed in a backscattering configuration using a Renishaw inVia Raman spectrometer equipped with a 532 nm excitation laser. This setup was utilized to investigate the potential formation of silicon clusters within the film. The inverse sheet resistance, herein called conductivity (σ) of the film, was measured using a custom-built system, with a mercury lamp calibrated to an intensity of one sun as light source.

RESULTS

Intrinsic a-SiC:H. To evaluate the suitability of 1−4-DB for producing an a-SiC:H layer, thin films were initially deposited at temperatures ranging from 500 to 600 °C, and their composition was analyzed using FTIR spectroscopy. FTIR

https://doi.org/10.1021/acsaelm.4c01992
ACS Appl. Electron. Mater. XXXX, XXX, XXX−XXX

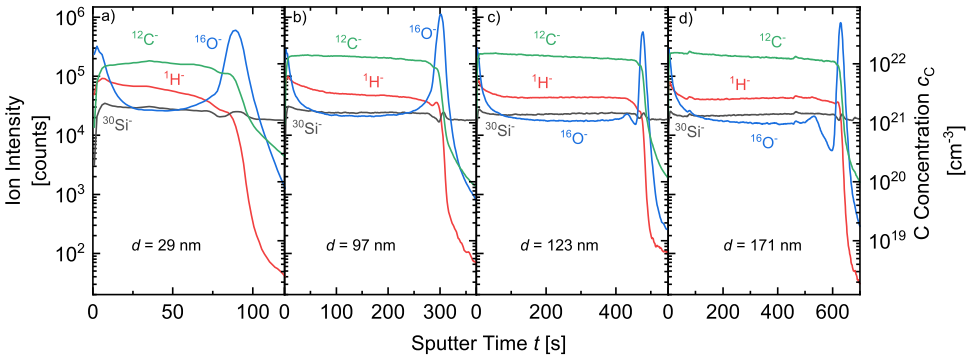

Figure 2. SIMS profile of a-SiC:H thin films deposited at (a) 530 °C, (b) 560 °C, (c) 585 °C, and (d) 600 °C. On the left y axis, the ion intensities of SIMS counts for H, Si, and O are given; the right y axis corresponds to the C concentration.

spectra around the characteristic IR peaks of a-SiC:H are shown in Figure 1.[13,16,17] In Figure 1a, mainly three modes contribute to the spectra: the Si−H wagging mode at 640 cm^{-1}, the SiC stretching mode in the range between 720 and 780 cm^{-1} and the Si−C−H$_x$ wagging modes around 980 cm^{-1}.[13,16−19] The Si−H mode at 640 cm^{-1} is strongly overlapped by the dominant SiC mode. The Si−C−H$_x$ wagging modes may overlap with Si−O$_x$ or Si−O−Si modes located at a similar wavelengths.[20,21] The broad SiC peak with a peak maximum located clearly below 780 cm^{-1} indicates, that the as deposited material is amorphous.[13,16] Figure 1b shows the Si−H stretching modes around 2100 cm^{-1}, and Figure 1c shows the C−H stretching modes at 2850 cm^{-1}.[13,18,22]

The C−H stretching peak at 2850 cm^{-1} increases proportionally with the peak at 980 cm^{-1}. This suggests that the 980 cm^{-1} peak is more likely due to Si−C−H$_x$ wagging modes rather than Si−O$_x$ and Si−O−Si modes. The ratio of the Si−C−H$_x$ wagging mode peak to the Si−C peak decreases as the deposition temperature increases. This indicates a lower amount of C−H$_x$ bonds within the film. In agreement with this, the ratio of the C−H stretching mode around 2850 cm^{-1} to the Si−H stretching mode around 2100 cm^{-1} decreases as well.

This trend is also shown in Figure 1d, which displays the densities of Si−C, Si−H, and C−H bonds in the films. Note that in contrast to the spectra shown in Figure 1a−c, which show the absorbance of the films, the calculation of the bond density takes into account the thickness of the film. These densities were calculated from their respective stretching vibrations as described in reference.[5] While the Si−C bond density increases with temperature, the Si−H and C−H bond densities decrease, with a steeper decrease for the C−H bond density.

The increase of the Si−C bond density with temperature indicates that c_C of the films increases as well. The observation is supported by the SIMS profiles in Figure 2. By comparing with a reference implant sample with a known c_C of 6×10^{19} cm^{-3} in the peak maximum, the average c_C within the a-SiC:H films was determined to 0.97×10^{22} cm^{-3} for T_d = 530 °C, 1.29×10^{22} cm^{-3} for T_d = 560 °C, 1.34×10^{22} cm^{-3} for T_d = 585 °C and 1.33×10^{22} cm^{-3} for T_d = 600 °C. The ionization cross section in SIMS strongly depends on the material and its structure. Due to the difference in c_C between the implantation standard and the samples, SIMS can only give a rough estimation of the absolute c_C. However, the c_C of $\sim 1.3 \times 10^{22}$ cm^{-3} for T_d = 585 and 600 °C roughly fits to a FTIR determined Si−C bond density of $\sim 8 \times 10^{22}$ cm^{-3} which corresponds to a c_C of 2×10^{22} cm^{-3} if fully bonded to silicon. On a logarithmic scale, the SIMS profiles indicate homogeneous film growth with minor changes in C, H, O and Si concentrations throughout the film thickness. Near the interface with the c-Si wafer as well as at the film surface, Figure 2 shows peaks in O intensity. The peak at the interface likely occurs due to native oxide on the c-Si substrate that was not removed prior to deposition. Oxygen at the film surface probably results from a native oxide layer often emerging when a-SiC:H films are exposed to ambient air.[23,24] However, on a linear scale, the c_C near the surface is higher than near the c-Si interface, possibly due to a gradual shift in the C radical to Si radical ratio within the deposition chamber atmosphere. The shift during deposition may occur due to a preferred Si than C incorporation, leading to a higher consumption of Si. This leads to c_C differences along the film thickness of ±25% compared to the average, disregarding surface or interface effects. The minimum and maximum values of c_C are given in Table 1.

Table 1. Minimum, Average, and Maximum Carbon Concentration c_C According to the SIMS Profiles

T_d [°C]	minimum c_C [10^{22} cm^{-3}]	average c_C [10^{22} cm^{-3}]	maximum c_C [10^{22} cm^{-3}]
530	0.69	0.97	1.12
560	1.09	1.29	1.41
585	1.16	1.34	1.52
600	1.09	1.33	1.63

The SIMS spectra in Figure 2 show that the O content is decreased with increasing deposition temperature. When compared with hydrogenated amorphous silicon (a-Si:H) deposited in the same system, as shown in Figure S3, all films exhibit relatively high O concentration, maybe caused by solvents within the precursor, or due to higher oxidation probability of C containing Si films.[23,24] A detailed analysis of the a-Si:H film shown in Figure S3 is presented in a separate report.[12] In the FTIR spectra in Figure 1, oxygen could not be distinctly detected, due to the overlap of Si−O$_x$ and Si−O−Si modes with the Si−C−H$_x$ modes. O is considered as an impurity within the a-SiC:H film, and its concentration within our films will be further addressed in the next chapter.

Crystallization of a-SiC:H. Crystallizing amorphous SiC films through annealing is a common step in the fabrication of solar cell devices such as TOPCon solar cells and all-silicon tandem solar cells.[5,25] To determine the optimal crystallization process, we used a-SiC:H films deposited at T_d = 585 °C and

https://doi.org/10.1021/acsaelm.4c01992
ACS Appl. Electron. Mater. XXXX, XXX, XXX−XXX

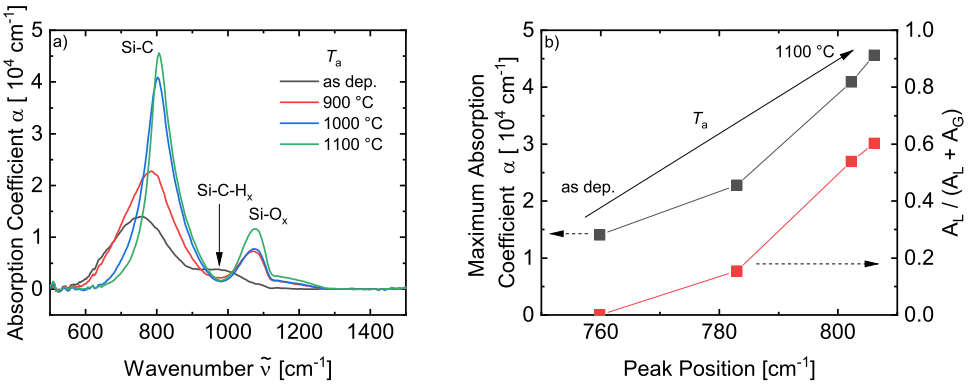

Figure 3. (a) FTIR spectra of SiC films as deposited and after annealing at 900, 1000, and 1100 °C. (b) Absorption coefficient maximum (left) and Lorentzian to Gaussian peak proportion ratio (right) of the Si−C stretching peak versus the SiC peak position. The increasing peak position with increasing annealing temperature is indicated with an arrow.

varied the annealing temperature T_a between 900 and 1100 °C. All of the annealed films were blistering-free. Figure 3 shows that already at T_a = 900 °C the SiC peak increases and shifts to higher wavenumbers, indicating a higher fraction of crystalline SiC within the film. Further increasing the temperature to 1000 °C significantly increases the peak height and shifts the peak maximum to wavenumbers above 800 cm^{-1}. This shift might be caused due to an overstoichiometric Si concentration within the film, as also observed by Weiss et al.[14] At 1100 °C, the absorption coefficient maximum further increases slightly to a value three times higher than that of the as-deposited film.

Crystallinity can be measured by the ratio of the Lorentzian to Gaussian peak contributions to the SiC stretching mode, shown in Figure 3b.[14] Similar to the peak height, the crystallinity increases with higher annealing temperatures, reaching a maximum of 60% at T_a = 1100 °C. A crystallinity below 100% for nonstoichiometric Si−C aligns with findings in ref 14 and may also be influenced by the relatively high O intensity within the films, as indicated by the SIMS measurements in Figure 2. For all annealing temperatures, H was completely effused from the films, as indicated by the disappearance of the 2100 cm^{-1} mode in the FTIR spectra (not shown). Besides changes in the Si−C peak, a new peak emerges around 1050 cm^{-1}, while the peak around 980 cm^{-1} vanishes. If the 980 cm^{-1} was due to Si−O$_x$ and Si−O−Si vibrations, its reduction could be explained by a shift to higher wavelengths due to the reordering of the Si−O$_x$ and Si−O−Si bonds.[26] These bonds would then contribute to the 1050 cm^{-1} peak shown in Figure 3a. However, we mainly attribute the 980 cm^{-1} peak to Si−C−H$_x$ vibrations due to its correlation with the C−H peak, as can be seen in Figure 1. Therefore, assuming the 980 cm^{-1} peak is attributed to Si−C−H$_x$ vibrations, an alternative explanation for the disappearance of the 980 cm^{-1} peak might be due to the restructuring of carbon within the crystals formed during the annealing and the effusion of H from the film. The appearance of the 1050 cm^{-1} peak might be not directly linked to the 980 cm^{-1} peak but rather results from the annealing process, as suggested by the SIMS profile of a sample annealed at 1100 °C, shown in Figure S1b. The profile reveals that most of the oxygen is concentrated on the surface of the film. This suggests that oxygen is incorporated during annealing from the surrounding atmosphere, which, although purged with nitrogen (N$_2$), is not fully evacuated before the process begins. As shown in Figure S2, most of this oxygen can be removed with an HF dip without etching any SiC. We therefore attribute the 980 cm^{-1} peak to Si−C−H$_x$ bonds and the 1050 cm^{-1} peak to Si−O$_x$ bonds. The absence of a significant Si−O$_x$ peak within the FTIR spectrum after the HF dip indicates that the oxygen content within the bulk of the film is less than 1%.

Since the FTIR and SIMS measurements on the amorphous material indicated an under stoichiometric silicon rich material, we used the Raman spectra, shown in Figure 4, to investigate

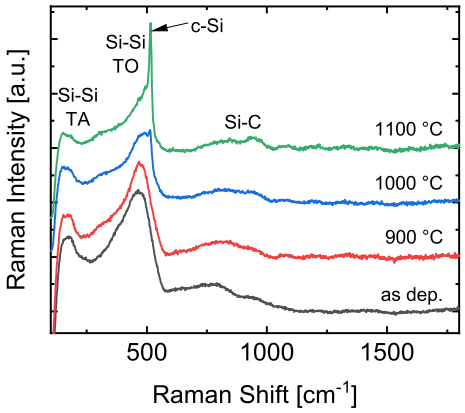

Figure 4. Raman spectra of SiC films as deposited and after annealing at 900, 1000, and 1100 °C. The corresponding bonding vibrations of the major peaks are indicated.

the formation of Si clusters within the films. A peak around 160 cm^{-1} probably resulting from transversal acoustic (TA) Si−Si modes, indicate the existence of a-Si within the film.[27] This is supported by a peak around 480 cm^{-1} occurring from transversal optical TO modes of a-Si. Note that the TO mode overlaps with Si−O modes from the substrate, which influence the peak height of the peak at 480 cm^{-1}.[28] The broad, weak signal between 700 and 1000 cm^{-1} can be assigned to Si−C vibrations.[7,29] In the same region second-order longitudinal optical (2LO) and second order TO modes of Si occur, which might overlap with the Si−C modes, which makes a clear classification difficult.[30] At a T_a of 1000 °C, a small peak at 520 cm^{-1} emerges, which gets stronger for T_a = 1100 °C. This clearly shows the formation of c-Si clusters within the SiC film. The fact, that this peak occurs only for $T_a \geq$ 1000 °C, indicates a substantial C concentration since the Si crystallization temperature increases with increasing C content.[29,31] Song et al.[29] found similar spectra for nonstoichiometric SiC.

https://doi.org/10.1021/acsaelm.4c01992
ACS Appl. Electron. Mater. XXXX, XXX, XXX−XXX

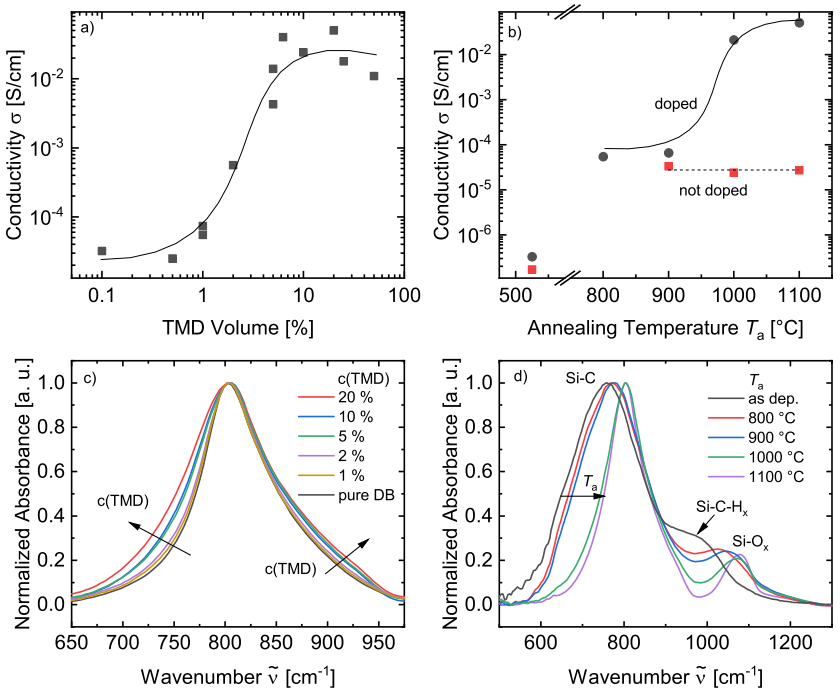

Figure 5. (a) Conductivity at T_a = 1100 °C crystallized SiC films vs the content of TMD diluted in DB used as a precursor. (b) Conductivity of undoped (red) and doped (gray) crystallized SiC films vs annealing temperature T_a. For the doped films, a precursor with 20% TMD was used. (c) FTIR spectra of Si−C modes within selected films of panel (a). (d) FTIR spectra of Si−C modes within the doped films also shown in panel (b).

Comparing the formation temperature of c-Si within the material of our films with the films in Song et al., yield a C concentration between 24 and 39%, in good agreement with the concentrations we found using FTIR spectroscopy.

Doped c-SiC. Knowing from Figure 3 that annealing at T_a = 1100 °C leads to the high crystallinity in the SiC samples, we used this temperature to crystallize doped SiC films. N is often used for doping in SiC.[6,32,33] To incorporate N into the films, we used liquid TMD mixed with DB as a precursor. Figure 5a shows the conductivity of the films after annealing at 1100 °C as a function of the TMD content within the precursor. By varying the TMD content, the conductivity can be adjusted over 3 orders of magnitude. Below 1% TMD content, no doping effect is observed in the SiC film. Between 1 and 5% TMD content, the conductivity sharply increases, indicating sufficient N is incorporation to dope the material. For higher TMD contents, the conductivity saturates at values up to 0.03 S cm^{-1}. This conductivity is within the typical range for crystalline, solar grade SiC doped with N.[34−36] Anwar et al.[37] reviewed several series of SiC samples with conductivities ranging from 10^{-9} to 10^{2} S cm^{-1}. The conductivities observed in the work presented here align well with this range and, spanning 5 orders of magnitude, cover a broader conductivity range than most other standalone material series. Besides nitrogen, oxygen is a typical additive to dope SiC films.[37,38] In Figure S4, we compare SIMS spectra of crystallized SiC films with (10% TMD) and without doping to investigate the changes in the nitrogen and oxygen content after doping. As a measure for the nitrogen content within the film, the SIMS-counts of $^{16}CN^-$ ions are given. Both spectra show a significant, but similar amount of oxygen. In contrast, the doped film shows 2 orders of magnitude increased SIMS-counts of $^{16}CN^-$ ions, indicating that the incorporation of nitrogen is the main reason for the increased conductivity of the films.

Increasing N concentration within the SiC films alters the chemical and electrical properties of the material, potentially shifting of the Si−C vibrational modes.[39,40] Figure 5c shows the normalized FTIR spectra of selected films from Figure 5a made with TMD contents between 1 and 20%, along with a spectrum of an as-deposited sample. With increasing TMD content in the precursor, the SiC peak broadens. The broadening to lower wavelengths might be caused by changes in the electrostatic environment of the Si−C bonds due to N inclusion or a higher amorphous SiC fraction resulting from N incorporation.[32] The broadening between 850 and 950 cm^{-1} of the peak is likely caused by emerging Si−N peaks located in this wavelength-regime, fitting to an increased N incorporation with higher TMD content.[32]

Figure 5b shows the dependence of the conductivity on T_a for undoped samples and samples doped with a precursor containing 20% TMD. The samples were deposited at a temperature of 585 °C, which is why the T_a of the as-deposited samples is set to 585 °C. As deposited, the doped and undoped samples exhibits similar conductivity of ∼2 × 10^{-7} S cm^{-1}, indicating that the introduced N is not active as a dopant. Annealing increases the conductivity of both undoped and doped SiC to almost 10^{-4} S cm^{-1}. This increase might be due to an increase in dangling bonds from H effusion or other restructuring of the SiC configuration, as indicated by a change in the FTIR peak position shown in Figure 5d. Further increasing the T_a does not change the conductivity of the undoped sample, even though a structural change from amorphous to crystalline SiC occurs, as shown in Figure 3 and the content of silicon nanocrystals (nc-Si) increases as shown in Figure 4. However, in contrast to the undoped samples, the transition from the amorphous to the crystalline phase in doped samples is accompanied by a significant increase in the conductivity up to 3 × 10^{-2} S cm^{-1}. This

https://doi.org/10.1021/acsaelm.4c01992
ACS Appl. Electron. Mater. XXXX, XXX, XXX−XXX

increase is most likely due to the activation of the N dopants within the crystalline SiC structure.

DISCUSSION

The study showed that liquid precursors, specifically 1,4-DB and 1,1,3,3-TMD, can be effectively used for SiC film deposition, including doping, at atmospheric pressure, offering a cost-effective and scalable alternative to traditional vacuum-based CVD methods. By using TMD we could achieve a significant incorporation of N into the films at deposition temperatures below 600 °C, which is lower than typical doping temperatures above 1000 °C when using N_2 or NH_3.[41,42] The FTIR spectra shown in Figure 1 show a dominant SiC stretching mode peak and a significant Si−C−H_x wagging modes peak typical for amorphous SiC and also found for a-SiC:H films made by PECVD.[13,23] The Si−C bonding density up to 8×10^{22} cm^{-3} and a H concentrations between 0.8 and 1.7×10^{22} cm^{-3} found in Figure 1 aligns perfectly with the density of a-SiC:H films reported by Kaneko et al.,[13] demonstrating the applicability of this process for the deposition of a-SiC:H films, which can be directly used as passivation layer in solar cells.[43] A further enhancement of the hydrogen content could potentially be achieved by increasing the growth rate.[12] However, the hydrogen content is inherently limited by the significant hydrogen effusion rates that occur at the elevated deposition temperatures required for the decomposition of DB. Figure 1d shows that especially for low deposition temperatures, there are more C−H than Si−H bonds within the a-SiC:H films. The higher ratio of C−H to Si−H vibrations for low deposition temperatures might be due to lower thermal energy, leading to less C−C bond breaking within the deposition process. The SIMS profiles in Figure 2 show an increase in C incorporation into the film with increasing growth duration. This might result from fewer Si atoms remaining in the precursor gas, leading to a higher amount of C radicals compared to Si radicals. This indicates that the Si to C ratio within the film can be adjusted by adding additional precursors containing only C−H complexes to increase the c_C within the film or only Si−H complexes to increase the Si concentration. The maximum average c_C of 1.34×10^{22} cm^{-3} (cf. Table 1) and a c_C of $\sim 2 \times 10^{22}$ cm^{-3} according to FTIR, indicates that the SiC is substoichiometric regarding the C content. However, since the reference sample had a c_C 3 orders of magnitude lower and since the density of the a-SiC:H films is unknown, estimating the absolute C to Si ratio is challenging. Annealing of the a-SiC:H films at 1000 and 1100 °C results in the formation of c-SiC as well as nc-Si clusters within the material, as shown in Figures 3 and 4. This aligns with existing literature and confirms the feasibility of the annealing process in enhancing the properties of the material.[1,5,32,44,45] The increase in conductivity from 2×10^{-5} to 0.03 S cm^{-1}, shown in Figure 5 for the films deposited using a mixture of >5% TMD in DB demonstrates the effectiveness of a liquid precursor for the incorporation of active dopants. This makes the resulting films suitable for electronic applications that require efficient charge carrier transport. The observed increase in conductivity is likely attributable to the formation of doped SiC or Si crystals. The most significant enhancement in conductivity occurred between annealing temperatures of 900 and 1000 °C, a range that coincides with substantial c-SiC formation as shown in Figure 3 and only minimal c-Si formation which increases for T_a = 1100 °C, as shown in Figure 4. This suggests that the doped c-SiC phase is the primary contributor to the observed conductivity improvements. This is supported by the fact that the N incorporation leads to a significant broadening of the SiC mode within the FTIR spectrum indicating N incorporation into the SiC matrix. Therefore, an optimization of the c-SiC content by using stoichiometric Si:C mixtures might be beneficial to further improve the conductivity for other semiconductor applications like transistors.[44,46]

A system allowing for higher deposition temperatures might enable higher c_C within the film. However, the current system is already at its limit, when operating at 600 °C. The use of other, carbon-rich precursors can also lead to higher C incorporation, but these precursors must match the decomposition temperature of DB. Further investigation is needed to find suitable precursors and their optimal mixing ratios with DB. Optimizing the N doping process could yield even higher conductivities, and exploring other dopants like aluminum may further enhance the properties of the film.[47] Additionally, a post-treatment for the incorporation of H might further increase the conductivity, making the film feasible for an application as a passivation layer in TOPCon solar cells.[5,48]

The FTIR spectrum after the HF dip in Figure S2, shows almost no Si−O peak, indicating an oxygen content of less than 1%. However, SIMS measurements, shown in Figure S3, reveal that a significant amount of oxygen is present in the films compared to a-Si films deposited in the same system. We attribute the higher oxygen content within the a-SiC:H films to three reasons: (i) The decomposition temperature of trisilane is lower than for disilabutane, which is why the ratio of the precursor radicals to oxygen impurity radicals is higher. This leads to fewer impurities within the film. (ii) In contrast to disilabutane, trisilane highly reacts with oxygen, forming solid silicon-oxide. This leads to self-purification of the process by reducing the O_2 content not only within the deposition chamber but within the whole glovebox. (iii) The purity of the trisilane precursor (>99.9%) is higher than for the disilabutane (99%). The lower purity might lead to a higher amount of O containing solvents, which are incorporated into the material during film growth. However, the exact composition of the remaining 1% of the precursor is not specified in the certificate of analysis document.

Regardless of its offspring, the unintentional incorporation of oxygen into the film can have significant effects on both the electrical and structural properties of the material. The acceptable amount of oxygen within the film depends on the application. Avila et al.[49] found significant structural changes of the material for oxygen contents >15%. The mechanical properties, however, can be changed significantly for lower O contents already.[50] For the application in electric devices, at grain boundaries and surfaces, oxygen can lead to the formation of SiO_2, an insulating phase that can interrupt conductive paths and thus reduce the overall conductivity of the SiC films. However, in small amounts, oxygen can also act as an (unintentional) dopant, influencing the charge carrier concentration.[37] While oxygen incorporation can potentially enhance certain properties of SiC films, careful control of its content is critical to maintaining the desired electrical and structural characteristics for electronic and photovoltaic applications. The SIMS analysis in Figure S4 used to detect and quantify both nitrogen and oxygen in the films show that after doping with TMD, the amount of O in the film is similar as within the film without doping. The amount of nitrogen however increased significantly, indicating that the increased

https://doi.org/10.1021/acsaelm.4c01992
ACS Appl. Electron. Mater. XXXX, XXX, XXX−XXX

conductivity indeed results from nitrogen doping instead of unintentional oxygen doping.

To reduce the O concentration due to solvents, precursors with a higher purity can be used, which might further enhance the conductivity. Additionally, the crystallization in a furnace with an evacuation system can increase the purity of the N_2 atmosphere, further reducing the O concentration within the film and preventing the formation of a SiO_x layer at the surface. Another possibility to reduce the O content is to increase T_d as indicated in Figure 2. The lower O content with increased T_d might result from higher amount of precursor radicals to impurity radicals.

a-SiC:H films with lower c_C than the films used for crystallization in this work are also utilized in nanoelectronic or optoelectronic devices. Reducing c_C lowers the crystallization temperature of nc-Si below that of SiC, potentially resulting in conductive nc-Si embedded within an a-SiC:H matrix, thereby enabling tunability of the optical bandgap.[1,3,7,31,45] This reduction in c_C can be readily achieved by decreasing the deposition temperature or by mixing 1,4-DB with a silicon-rich precursor like trisilane, making the process suitable for the deposition of films designed for the formation of nc-Si within an a-SiC:H matrix.

The APCVD method for the SiC film deposition reduces operational costs and simplifies the scaling process, making it feasible for large-scale manufacturing. The structural integrity and electrical properties of these films make them promising candidates for applications requiring high thermal stability and efficient charge transport, such as TOPCon solar cells and all-silicon tandem solar cells.

CONCLUSIONS

This study highlights the potential of using liquid precursors for SiC film deposition at atmospheric pressure, by successfully depositing N containing a-SiC:H films with carbon contents of 1×10^{22}–2×10^{22} cm^{-3} using liquid DB and TMD at temperatures below 600 °C and subsequent crystallization and dopant activation. We found a minimum temperature of 1000 °C for the formation of SiC crystals. Higher temperatures increase the proportion of crystalline material. The phase transition from undoped amorphous to crystalline material itself leads to a conductivity increase from 2×10^{-7} S cm^{-1} to almost 10^{-4} S cm^{-1}. Crystallizing N containing a-SiC:H films facilitate even higher improvements in electrical conductivity, achieving values as high as 0.03 S cm^{-1}. These enhancements are attributed to the effective incorporation of nitrogen atoms into the crystalline SiC matrix, which effectively tunes the electronic structure and enhances charge carrier mobility.

This work thus provides a cost-effective, scalable, and high-performance solution for advanced electronic and photovoltaic applications. A significant challenge for scalability lies in achieving a uniform temperature distribution across the substrate and ensuring consistent precursor delivery. Incorporating Si-rich or C-rich precursors could help expand the range of adjustable Si/C ratios, which in this study was primarily controlled through variations in deposition temperature. To achieve SiC films with high purity and exceptionally low oxygen content (≪0.1%), it may be necessary to purify the precursor and lower the oxygen concentration within the glovebox to below 1 ppm. With further optimization and research, the approach presented within this work could significantly advance the manufacturing and application of a-SiC:H, c-SiC, and nc-Si/a-SiC:H films in various high-tech industries, especially with respect to the application in TOPCon solar cells.

ASSOCIATED CONTENT

Supporting Information

The Supporting Information is available free of charge at https://pubs.acs.org/doi/10.1021/acsaelm.4c01992.

SIMS profiles and FTIR spectra, including annealing effects, HF etching effects, hydrogen and oxygen concentrations, and comparison of doped and undoped films (PDF)

AUTHOR INFORMATION

Corresponding Author

Benedikt Fischer − *IMD-3 Photovoltaik, Forschungszentrum Jülich GmbH, 52425 Jülich, Germany; Jülich Aachen Research Alliance (JARA-Energy) and Faculty of Electrical Engineering and Information Technology, RWTH Aachen University, 52062 Aachen, Germany;* orcid.org/0000-0002-4315-8110; Email: b.fischer@fz-juelich.de

Authors

Maurice Nuys − *IMD-3 Photovoltaik, Forschungszentrum Jülich GmbH, 52425 Jülich, Germany; Department of Energy Building Services Environmental Engineering, University of Applied Sciences Muenster, 48565 Steinfurt, Germany*

Stefan Haas − *IMD-3 Photovoltaik, Forschungszentrum Jülich GmbH, 52425 Jülich, Germany; Department of Aerospace Engineering, FH Aachen University of Applied Sciences, 52066 Aachen, Germany*

Oliver Thimm − *IMD-3 Photovoltaik, Forschungszentrum Jülich GmbH, 52425 Jülich, Germany*

Gunnar Schöpe − *IMD-3 Photovoltaik, Forschungszentrum Jülich GmbH, 52425 Jülich, Germany*

Pascal Foucart − *IMD-3 Photovoltaik, Forschungszentrum Jülich GmbH, 52425 Jülich, Germany*

Astrid Besmehn − *IET-4 Elektrochemische Verfahrenstechnik, Forschungszentrum Jülich GmbH, 52425 Jülich, Germany*

Uwe Rau − *IMD-3 Photovoltaik, Forschungszentrum Jülich GmbH, 52425 Jülich, Germany; Jülich Aachen Research Alliance (JARA-Energy) and Faculty of Electrical Engineering and Information Technology, RWTH Aachen University, 52062 Aachen, Germany*

Complete contact information is available at: https://pubs.acs.org/10.1021/acsaelm.4c01992

Author Contributions

The research project was a collaborative effort, with each author contributing to specific roles. B.F. and M.N. jointly conceptualized the study design and defined the research objectives. Data curation was conducted by B.F., who collected, organized, and curated the data for subsequent analysis. B.F. took charge of the formal analysis interpreting the results alongside M.N. Securing the funding necessary to execute the research was the responsibility of U.R., S.H., and M.N., who successfully acquired the financial resources. The investigation phase was led by B.F., O.T., G.S., and A.B., who oversaw the experiments and investigations outlined in the study. Methodological frameworks and experimental protocols were developed by B.F. in collaboration with M.N. Project administration duties were shared among all authors, with B.F. coordinating and managing the overall project workflow. The

https://doi.org/10.1021/acsaelm.4c01992
ACS Appl. Electron. Mater. XXXX, XXX, XXX−XXX

provision of essential resources for the research was ensured by U.R. and S.H. M.N., S.H., and U.R. provided supervision, offering guidance throughout the project lifecycle. Visual representations of the data and results were created by B.F. and P.F. The initial version of the manuscript was drafted by B.F., with subsequent critical reviews and editing conducted by all authors to refine the intellectual content and enhance clarity.

Funding

This work was funded by Forschungszentrum Juelich GmbH.

Notes

The authors declare no competing financial interest.

REFERENCES

(1) Coscia, U.; Ambrosone, G.; Lettieri, S.; Maddalena, P.; Ferrero, S. Microcrystalline Silicon−Carbon Films Deposited by Silane−Methane Mixture Highly Diluted in Hydrogen. *Thin Solid Films* **2006**, *511−512*, 399−403.

(2) Cheng, C.-H.; Wu, C.-L.; Lin, Y.-H.; Yan, W.-L.; Shih, M.-H.; Chang, J.-H.; Wu, C.-I.; Lee, C.-K.; Lin, G.-R. Strong Optical Nonlinearity of the Nonstoichiometric Silicon Carbide. *J. Mater. Chem. C* **2015**, *3* (39), 10164−10176.

(3) Shan, D.; Sun, D.; Tang, M.; Yang, R.; Kang, G.; Tao, T.; Cao, Y. Structures, Electronic Properties and Carrier Transport Mechanisms of Si Nano-Crystalline Embedded in the Amorphous SiC Films with Various Si/C Ratios. *Nanomaterials* **2021**, *11* (10), 2678.

(4) Steinhauser, B.; Feldmann, F.; Polzin, J.-I.; Tutsch, L.; Arya, V.; Grübel, B.; Fischer, A.; Moldovan, A.; Benick, J.; Richter, A.; Brand, A. A.; Kluska, S.; Hermle, M. Large Area TOPCon Technology Achieving 23.4% Efficiency. In *2018 IEEE 7th World Conference on Photovoltaic Energy Conversion (WCPEC) (A Joint Conference of 45th IEEE PVSC, 28th PVSEC & 34th EU PVSEC)*; IEEE: Waikoloa, HI, USA, 2018; 1507−1510.

(5) Xu, Z.; Tao, K.; Jiang, S.; Jia, R.; Li, W.; Zhou, Y.; Jin, Z.; Liu, X. Application of Polycrystalline Silicon Carbide Thin Films as the Passivating Contacts for Silicon Solar Cells. *Sol. Energy Mater. Sol. Cells* **2020**, *206*, No. 110329.

(6) Köhler, M.; Pomaska, M.; Procel, P.; Santbergen, R.; Zamchiy, A.; Macco, B.; Lambertz, A.; Duan, W.; Cao, P.; Klingebiel, B.; Li, S.; Eberst, A.; Luysberg, M.; Qiu, K.; Isabella, O.; Finger, F.; Kirchartz, T.; Rau, U.; Ding, K. A Silicon Carbide-Based Highly Transparent Passivating Contact for Crystalline Silicon Solar Cells Approaching Efficiencies of 24%. *Nat. Energy* **2021**, *6* (5), 529−537.

(7) Wan, Z.; Huang, S.; Green, M. A.; Conibeer, G. Rapid Thermal Annealing and Crystallization Mechanisms Study of Silicon Nanocrystal in Silicon Carbide Matrix. *Nanoscale Res. Lett.* **2011**, *6* (1), 129.

(8) Gou, L.; Qi, C.; Ran, J.; Zheng, C. SiC Film Deposition by DC Magnetron Sputtering. *Thin Solid Films* **1999**, *345*, 42−44.

(9) Kern, R. S.; Järrendahl, K.; Tanaka, S.; Davis, R. F. Homoepitaxial SiC Growth by Molecular Beam Epitaxy. *phys. stat. sol. (b)* **1997**, *202* (1), 379−404.

(10) Okada, L. A.; Dillon, A. C.; Ott, A. W.; George, S. M. Adsorption and Decomposition of 1,4-Disilabutane (SiH3CH2CH2-SiH3) on Si(100) 2 × 1 and Porous Silicon Surfaces. *Surf. Sci.* **1998**, *418* (2), 353−366.

(11) Abyzov, A. M.; Smirnov, E. P. Kinetics of SiC Chemical Vapor Deposition from Methylsilane. *Inorg. Mater.* **2000**, *36* (9), 884−890.

(12) Fischer, B.; Nuys, M.; Astakhov, O.; Haas, S.; Schaaf, M.; Besmehn, A.; Jakes, P.; Eichel, R.-A.; Rau, U. Advanced Atmospheric Pressure CVD of A-Si:H Using Pure and Cyclooctane-Diluted Trisilane as Precursors. *Sustain. Energy Fuels* **2024**, *8*, 5568.

(13) Kaneko, T.; Nemoto, D.; Horiguchi, A.; Miyakawa, N. FTIR Analysis of A-SiC:H Films Grown by Plasma Enhanced CVD. *J. Cryst. Growth* **2005**, *275* (1−2), e1097−e1101.

(14) Weiss, C.; Schnabel, M.; Reichert, A.; Löper, P.; Janz, S. Structural and Optical Properties of Silicon Nanocrystals Embedded in Silicon Carbide: Comparison of Single Layers and Multilayer Structures. *Appl. Surf. Sci.* **2015**, *351*, 550−557.

(15) Heera, V.; Prokert, F.; Schell, N.; Seifarth, H.; Fukarek, W.; Voelskow, M.; Skorupa, W. Density and Structural Changes in SiC after Amorphization and Annealing. *Appl. Phys. Lett.* **1997**, *70* (26), 3531−3533.

(16) Kim, D. S.; Lee, Y. H. Room-Temperature Deposition of a-SiC:H Thin Films by Ion-Assisted Plasma-Enhanced CVD. *Thin Solid Films* **1996**, *283* (1), 109−118.

(17) King, S. W.; French, M.; Bielefeld, J.; Lanford, W. A. Fourier Transform Infrared Spectroscopy Investigation of Chemical Bonding in Low-k a-SiC:H Thin Films. *J. Non-Cryst. Solids* **2011**, *357* (15), 2970−2983.

(18) Brodsky, M. H.; Cardona, M.; Cuomo, J. J. Infrared and Raman Spectra of the Silicon-Hydrogen Bonds in Amorphous Silicon Prepared by Glow Discharge and Sputtering. *Phys. Rev. B* **1977**, *16* (8), 3556−3571.

(19) Vetter, M. IR-Study of a-SiCx:H and a-SiCxNy:H Films for c-Si Surface Passivation. *Thin Solid Films* **2004**, *451−452*, 340−344.

(20) Lucovsky, G. A Structural Interpretation of the Infrared Absorption Spectra of A-Si:H:O Alloys. *Solar Energy Materials* **1982**, *8* (1−3), 165−175.

(21) Zamchiy, A. O.; Baranov, E. A.; Merkulova, I. E.; Khmel, S. Ya.; Maximovskiy, E. A. Determination of the Oxygen Content in Amorphous SiOx Thin Films. *J. Non-Cryst. Solids* **2019**, *518*, 43−50.

(22) Beyer, W.; Ghazala, M. S. A. Absorption Strengths of Si-H Vibrational Modes in Hydrogenated Silicon. *MRS Proc.* **1998**, *507*, 601.

(23) Huran, J.; Boháček, P.; Sasinková, V.; Kleinová, A.; Mikolášek, M.; Kobzev, A. P. Amorphous Silicon Carbide Thin Films Doped with P or B for the Photoelectrochemical Water Splitting Devices. *Curr. Appl. Phys.* **2022**, *34*, 101−106.

(24) Moll, P.; Pfusterschmied, G.; Schwarz, S.; Stöger-Pollach, M.; Schmid, U. Impact of Alternating Precursor Supply and Gas Flow on the LPCVD Growth Behavior of Polycrystalline 3C-SiC Thin Films on Si. *Sensors and Actuators A: Physical* **2024**, *372*, No. 115376.

(25) Qiu, K.; Pomaska, M.; Li, S.; Lambertz, A.; Duan, W.; Gad, A.; Geitner, M.; Brugger, J.; Liang, Z.; Shen, H.; Finger, F.; Rau, U.; Ding, K. Development of Conductive SiCx:H as a New Hydrogenation Technique for Tunnel Oxide Passivating Contacts. *ACS Appl. Mater. Interfaces* **2020**, *12* (26), 29986−29992.

(26) Yi, L. X.; Heitmann, J.; Scholz, R.; Zacharias, M. Phase Separation of Thin SiO Layers in Amorphous SiO/SiO $_2$ Superlattices during Annealing. *J. Phys.: Condens. Matter* **2003**, *15* (39), S2887−S2895.

(27) Belrhiti Alaoui, K.; Laalioui, S.; Naimi, Z.; Ikken, B.; Outzourhit, A. Photovoltaic and Impedance Spectroscopy Characterization of Single-Junction a-Si:H p−i−n Solar Cells Deposited by Simple Shadow Masking Techniques Using PECVD. *AIP Advances* **2020**, *10* (9), No. 095315.

(28) Krishnan, R. S. Raman Spectra of the Second Order in Crystals. *Proc. Indian Acad. Sci.* **1945**, *22* (5), 329.

(29) Song, D.; Cho, E.-C.; Cho, Y.-H.; Conibeer, G.; Huang, Y.; Huang, S.; Green, M. A. Evolution of Si (and SiC) Nanocrystal Precipitation in SiC Matrix. *Thin Solid Films* **2008**, *516* (12), 3824−3830.

(30) Spizzirri, P. G.; Fang, J.-H.; Rubanov, S.; Gauja, E.; Prawer, S. Nano-Raman Spectroscopy of Silicon Surfaces. *arXiv*, 2010.

(31) Song, D.; Cho, E.-C.; Conibeer, G.; Huang, Y.; Flynn, C.; Green, M. A. Structural Characterization of Annealed Si1−xCx/SiC Multilayers Targeting Formation of Si Nanocrystals in a SiC Matrix. *J. Appl. Phys.* **2008**, *103* (8), No. 083544.

(32) Weiss, C.; Schnabel, M.; Prucnal, S.; Hofmann, J.; Reichert, A.; Fehrenbach, T.; Skorupa, W.; Janz, S. Formation of Silicon Nanocrystals in Silicon Carbide Using Flash Lamp Annealing. *J. Appl. Phys.* **2016**, *120* (10), 105103.

(33) Eberst, A.; Zamchiy, A.; Qiu, K.; Winkel, P.; Gebrewold, H. T.; Lambertz, A.; Duan, W.; Li, S.; Bittkau, K.; Kirchartz, T.; Rau, U.; Ding, K. Optical Optimization Potential of Transparent-Passivated Contacts in Silicon Solar Cells. *Solar RRL* **2022**, *6* (6), No. 2101050.

https://doi.org/10.1021/acsaelm.4c01992
ACS Appl. Electron. Mater. XXXX, XXX, XXX−XXX

(34) Eberst, A.; Lambertz, A.; Duan, W.; Smirnov, V.; Rau, U.; Ding, K. Material Properties of Nanocrystalline Silicon Carbide for Transparent Passivating Contact Solar Cells. *Solar RRL* **2023**, *7* (7), No. 2300013.
(35) Xiao, L.; Astakhov, O.; Carius, R.; Chen, T.; Wang, H.; Stutzmann, M.; Finger, F. Paramagnetic States in Mc-SiC:H Thin Films Prepared by Hot-Wire CVD at Low Temperatures. *Phys. Status Solidi (c)* **2010**, *7* (3−4), 778−781.
(36) Demichelis, F.; Pirri, C. F.; Tresso, E. Microcrystallization Formation in Silicon Carbide Thin Films. *Philosophical Magazine B* **1992**, *66* (1), 135−146.
(37) Anwar, M. S.; Bukhari, S. Z. A.; Ha, J.-H.; Lee, J.; Song, I.-H.; Kim, Y.-W. Controlling the Electrical Resistivity of Porous Silicon Carbide Ceramics and Their Applications: A Review. *International Journal of Applied Ceramic Technology* **2022**, *19* (4), 1814−1840.
(38) Pomaska, M.; Mock, J.; Köhler, F.; Zastrow, U.; Perani, M.; Astakhov, O.; Cavalcoli, D.; Carius, R.; Finger, F.; Ding, K. Role of Oxygen and Nitrogen in N-Type Microcrystalline Silicon Carbide Grown by Hot Wire Chemical Vapor Deposition. *J. Appl. Phys.* **2016**, *120* (22), 225105.
(39) Huran, J.; Valovič, A.; Kučera, M.; Kleinová, A.; Kovaččová, E.; Boháček, P.; Sekáčová, M. Hydrogenated Amorphous Silicon Carbon Nitride Films Prepared by PECVD Technology: Properties. *Journal of Electrical Engineering* **2012**, *63* (5), 333−335.
(40) Fainer, N. I.; Plekhanov, A. G.; Golubenko, A. N.; Rumyantsev, Y. M.; Rakhlin, V. I.; Maximovski, E. A.; Shayapov, V. R. PECVD Synthesis of Silicon Carbonitride Layers Using Methyltris-(Diethylamino)Silane as the New Single-Source Precursor. *ECS J. Solid State Sci. Technol.* **2015**, *4* (1), N3153.
(41) Liu, F.; Carraro, C.; Pisano, A. P.; Maboudian, R. Growth and Characterization of Nitrogen-Doped Polycrystalline 3C-SiC Thin Films for Harsh Environment MEMS Applications. *J. Micromech. Microeng.* **2010**, *20* (3), No. 035011.
(42) Krötz, G.; Möller, H.; Eickhoff, M.; Zappe, S.; Ziermann, R.; Obermeier, E.; Stoemenos, J. Heteroepitaxial Growth of 3C-SiC on SOI for Sensor Applications. *Materials Science and Engineering: B* **1999**, *61−62*, 516−521.
(43) Boccard, M.; Holman, Z. C. Amorphous Silicon Carbide Passivating Layers for Crystalline-Silicon-Based Heterojunction Solar Cells. *J. Appl. Phys.* **2015**, *118* (6), No. 065704.
(44) Calcagno, L.; Musumeci, P.; Roccaforte, F.; Bongiorno, C.; Foti, G. Crystallisation Mechanism of Amorphous Silicon Carbide. *Appl. Surf. Sci.* **2001**, *184* (1), 123−127.
(45) Kar, D.; Das, D. Conducting Wide Band Gap Nc-Si/a-SiC:H Films for Window Layers in Nc-Si Solar Cells. *Journal of Materials Chemistry A* **2013**, *1* (46), 14744−14753.
(46) Wijesundara, M. B. J.; Stoldt, C. R.; Carraro, C.; Howe, R. T.; Maboudian, R. Nitrogen Doping of Polycrystalline 3C−SiC Films Grown by Single-Source Chemical Vapor Deposition. *Thin Solid Films* **2002**, *419* (1−2), 69−75.
(47) Xiao, L.; Astakhov, O.; Chen, T.; Stutzmann, M.; Finger, F. Aluminum Doped Silicon Carbide Thin Films Prepared by Hot-Wire CVD: Investigation of Defects with Electron Spin Resonance. *Thin Solid Films* **2011**, *519* (14), 4519−4522.
(48) Zheng, J.; Yang, Z.; Lu, L.; Feng, M.; Zhi, Y.; Lin, Y.; Liao, M.; Zeng, Y.; Yan, B.; Ye, J. Blistering-Free Polycrystalline Silicon Carbide Films for Double-Sided Passivating Contact Solar Cells. *Sol. Energy Mater. Sol. Cells* **2022**, *238*, No. 111586.
(49) Avila, A.; Montero, I.; Galán, L.; Ripalda, J. M.; Levy, R. Behavior of Oxygen Doped SiC Thin Films: An x-Ray Photoelectron Spectroscopy Study. *J. Appl. Phys.* **2001**, *89* (1), 212−216.
(50) Feng, D.; Ren, Q.; Ru, H.; Wang, W.; Jiang, Y.; Ren, S.; Zhang, C. Effect of Oxygen Content on the Sintering Behaviour and Mechanical Properties of SiC Ceramics. *Ceram. Int.* **2019**, *45* (18), 23984−23992.

https://doi.org/10.1021/acsaelm.4c01992
ACS Appl. Electron. Mater. XXXX, XXX, XXX−XXX